

PAMELA and dark matter

V. Barger¹, W.-Y. Keung², D. Marfatia³, G. Shaughnessy^{1,4,5}

¹*Department of Physics, University of Wisconsin, Madison, WI 53706*

²*Department of Physics, University of Illinois, Chicago, IL 60607*

³*Department of Physics and Astronomy, University of Kansas, Lawrence, KS 66045*

⁴*Department of Physics and Astronomy, Northwestern University, Evanston, IL 60208 and*

⁵*High Energy Physics Division, Argonne National Laboratory, Argonne, IL 60439*

Assuming that the positron excess in PAMELA satellite data is a consequence of annihilations of cold dark matter, we consider from a model-independent perspective if the data show a preference for the spin of dark matter. We then perform a general analysis of annihilations into two-body states to determine what weighted combination of channels best describes the data.

Introduction. One of the unsolved problems in cosmology and particle physics is the nature of dark matter (DM) which accounts for about 20% of the energy density of the universe. Particle physics models typically relate discrete symmetries with the existence of a stable cold DM candidate. A variety of such models have been suggested that provide viable explanations of the DM. Weakly interacting massive particles (WIMPs) can be either of integer or noninteger spin. The classic case of supersymmetry (SUSY) has a spin-1/2 neutralino as dark matter whereas extra dimensional models and collective symmetry breaking models have spin-1 dark matter. Specific realizations are the minimal Universal Extra Dimensions (mUED) [1] and Little Higgs with T-parity (LHT) [2] models. Spin-0 dark matter is possible in models with an additional singlet in the scalar sector of the Standard Model [3].

Recent evidence for a positron excess in the Payload for Matter Antimatter Exploration and Light-nuclei Astrophysics (PAMELA) data [4] spurs attention to WIMPs whose annihilations in the galactic halo can explain an excess over backgrounds [5, 6]. PAMELA data presented thus far show a turn-up in the energy spectrum at about 10 GeV and a steady rise up to 100 GeV with no fall-off in that dataset.¹ The shape of the spectrum bears directly on the annihilation mechanism. Spin-1 DM annihilations directly into e^+e^- produce a line spectrum, whereas spin-1/2 Majorana DM will give a continuum spectrum from secondary decays of weak bosons, quarks and leptons.

Our goals are to study in a model-independent approach if the PAMELA excess provides hints about the spin of the DM particle and what annihilation channels are favored by the data. We do not subscribe to any specific particle physics model, but comment on models where appropriate. We also do not require that the measured relic abundance be reproduced since this is highly model-dependent. Moreover, the total energy density in dark matter may be comprised of several components,

so only an upper bound need be imposed on the energy density of a particular DM particle. The nature of our analysis precludes us from making projections for signatures at IceCube, the Fermi Gamma-ray Space Telescope, direct detection experiments and the Large Hadron Collider, all of which are interesting in their own right.

Modelling the positron signal and background.

The positron background expected primarily from supernovae and from collisions of cosmic ray protons and nuclei on the interstellar medium is simulated in Ref. [8]. The results of the simulation have the convenient parameterization [9], $\Phi_{e^+}^{bkg} = 4.5E^{0.7}/(1 + 650E^{2.3} + 1500E^{4.2})$, with the energy of the positron E in GeV. Since we present our results as a positron fraction $\Phi_{e^+}/(\Phi_{e^+} + \Phi_{e^-})$ which allows for cancellations of systematic uncertainties and the effects of solar activity, we also need the electron background which is analogously parameterized by [10] $\Phi_{e^-}^{bkg} = 0.16E^{-1.1}/(1 + 11E^{0.9} + 3.2E^{2.15}) + 0.7E^{0.7}/(1 + 110E^{1.5} + 580E^{4.2})$. Solar modulations arise from the phase of the solar cycle and from the opposite charges of electrons and positrons. Without charge sign bias, the positron ratio is independent of solar activity. However, since PAMELA data show evidence of charge sign dependence for positron energies below 10 GeV, we only analyze data above 10 GeV.

Positrons produced in DM annihilations propagate through the interstellar medium to the earth and as a consequence suffer absorption effects that broaden the positron spectrum to lower energies. We estimate the primary positron flux from dark matter annihilations according to the prescription of Refs. [10, 11, 12]. Here we briefly describe the procedure and refer the reader to Refs. [10, 12] for details.

The positron number density per unit energy is governed by the diffusion-loss equation with diffusion coefficient $K(E) = K_0(E/\text{GeV})^\delta$ which describes propagation through turbulent magnetic fields, and is taken to be independent of position. The equation also accounts for energy losses through synchrotron radiation and inverse Compton scattering on the cosmic microwave background and infrared galactic starlight. The diffusion zone in which the diffusion-loss equation is applicable is modelled as a cylinder of height $2L$ and radius 20 kpc that straddles the galactic plane in which most cosmic ray in-

¹ We do not consider the excess in the $e^+ + e^-$ energy spectrum between 500 and 800 GeV seen by the PPB-BETS balloon experiment [7].

Model	δ	K_0 (kpc ² /Myr)	L (kpc)
Min	0.55	0.00595	1
Med	0.70	0.0112	4
Max	0.46	0.0765	15

TABLE I: Three sets of parameters describing cosmic ray propagation [12]. The Med set is the best-fit to the measured boron to carbon ratio. The Min and Max sets minimize and maximize the positron fluxes above 10 GeV, respectively.

teractions take place. The positron number density is assumed to vanish on the surface of the cylinder, since outside the diffusion zone the positrons propagate freely and escape into the intergalactic medium. The source of the positrons due to DM annihilations depends on the DM density profile and on the annihilation cross section. For the former, we adopt a cored isothermal halo profile [13].

The normalization K_0 and the spectral index δ of the diffusion coefficient, and L can all be selected to be consistent with the measured boron to carbon ratio in cosmic rays [14]. We consider three sets of these parameters, “Min”, “Med” and “Max”, of Ref. [12] and reproduce them in Table I. The Med set has values of K_0 , δ and L which best fit the measured boron to carbon ratio. The Min and Max sets minimize and maximize the positron fluxes above about 10 GeV. Needless to say, the Min and Max sets are only representative, since the positron flux depends on the mass of the DM particle M_{DM} and on the annihilation channel once the halo profile is selected.

Assuming steady-state conditions, a semi-analytic expression for the primary positron flux has been obtained [11, 12]. The result depends on a so-called “halo function” which encodes the physics of cosmic ray propagation. We employ numerical fit functions [10] for the halo functions pertinent to the isothermal profile with the Min, Med and Max propagation parameter sets. We allow for the possibility of high density substructures in the dark matter halo that enhance the positron flux by an energy-independent “boost factor” B . Note that N -body simulations suggest that B can not be larger than about 10 and may be energy-dependent [15].

Dark matter annihilations and spin. To begin with, we assume M_{DM} is smaller than the top quark mass. This choice is dictated by our interest in model-independence. (We shall see later, by extending the range of M_{DM} , that the positron data typically select DM lighter than the top quark for the Med set). If the $t\bar{t}$ channel were open, the relative contributions of different channels to the positron spectrum would depend on the details of the Higgs sector.

Since the PAMELA data show a sharp rise, we initially only consider positrons from a e^+ line spectrum or from the two-body decays of pair-produced weak bosons at the source. Specifically, we study the spectra from direct production, $DMDM \rightarrow e^+e^-$ (which produces a positron line close to M_{DM}), and from secondary produc-

spin	s -channel Higgs	t, u -channel fermion	t, u -channel boson
0	LL, TT	X	LL
$\frac{1}{2}$	0	TT	X
1	LL, TT	X	LL, TT

TABLE II: Polarizations of W pairs produced by static annihilations $DMDM \rightarrow W^+W^-$ depend on the spin of the DM particle. “LL” and “TT” indicate that the W bosons are longitudinally and transversely polarized, respectively. “X” indicates that there is no contribution at the tree-level, and “0” indicates that the amplitude vanishes in the static limit. Note that Dirac fermion DM also has contributions from s -channel Z -exchange.

tion from the process $DMDM \rightarrow W^+W^-$.² Concrete examples of direct annihilation into e^+e^- are found in mUED and LHT in which spin-1 DM annihilate by exchange of an odd-parity fermion [16, 17]. Direct annihilation also occurs for hidden/mirror Dirac fermions and sterile neutrinos. The latter constitute warm DM which is not relevant to our study of nonrelativistic DM. If DM is a Majorana fermion, helicity suppression prevents the direct production of e^+e^- . For scalar DM the amplitude for static annihilation into light fermions vanishes [18]. Since the production of W pairs is spin-dependent, we further classify the positron spectra according to whether the W bosons are longitudinally polarized or transversely polarized.

The normalized distributions for the e^+ energy are

$$f_{TT}(x) = 3 \frac{\beta_W^2 + (1-x)^2}{8\beta_W^3} \quad (1)$$

$$f_{LL}(x) = 3 \frac{\beta_W^2 - (1-x)^2}{4\beta_W^3}, \quad (2)$$

for the WW transverse (TT) modes and longitudinal (LL) mode, respectively, where $\beta_W^2 = 1 - m_W^2/M_{DM}^2$ and $x = 2E_{e^+}/M_{DM} \lesssim 1 \pm \beta_W$. In general, if the W^+W^- channel has both TT and LL contributions of relative weights a and b , then the resultant distribution which combines two TT modes and one LL mode is $(af_{LL}(x) + bf_{TT}(x))/(a+b)$.

In Table II, we categorize the polarization modes of the W pair according to the spin of the DM particle. While fermionic DM can not annihilate into W pairs via s -channel Higgs exchange in the static limit, spin-0 and spin-1 DM annihilations (with relative weights $a = (1 + \beta_W^2)^2$ and $b = 2(1 - \beta_W^2)^2$) give the distribution,

$$\frac{1}{N} \frac{dN}{dx} = \frac{3[1 + \beta_W^4 - 2(1-x)^2]}{2\beta_W(3 - 2\beta_W^2 + 3\beta_W^4)}. \quad (3)$$

² Although each Z in a Z pair produces a positron, since $\sigma(DMDM \rightarrow W^+W^-)/\sigma(DMDM \rightarrow ZZ) \approx 2$ in the high-energy limit, and since the leptonic branching fraction for W s is three times as much as for Z s, W pairs produce three times as many positrons as Z pairs with almost identical distributions.

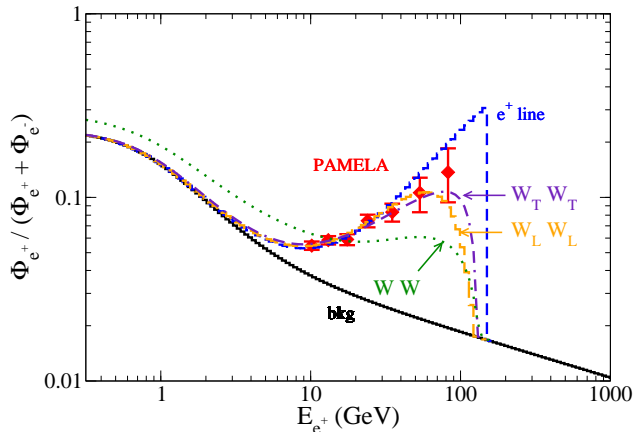


FIG. 1: Annihilations of DM directly into e^+e^- give the e^+ line at about $M_{DM} = 150$ GeV. The secondary positron spectrum from decays into $e^+\nu$ of longitudinal (transverse) W bosons is labeled $W_L W_L$ ($W_T W_T$); the soft component of the spectra are neglected for illustration. Including the soft component (with spin-correlations neglected) results in a much softer spectrum labelled WW that does not fit the PAMELA data above 10 GeV. The solid curve is the expected background. The Med set of propagation parameters is used with a cored isothermal profile for the DM halo.

Note that as $\beta_W \rightarrow 1$, the longitudinal mode dominates. The DM particle in both mUED and LHT can annihilate via s -channel Higgs exchange. Whether these models produce line or continuum spectra or both depends on specific realizations.

Fermionic DM annihilations via t - or u - exchange of a fermion give only TT modes. The positron spectrum is then simply $f_{TT}(x)$ [19]. SUSY provides the common example of neutralinos that annihilate dominantly by t - and u -channel chargino exchange.

Analysis. In Fig. 1, we show spectral distributions of positrons produced in annihilations of a DM particle of mass 150 GeV that fit the PAMELA excess. We have assumed that when direct production occurs, annihilations into W^+W^- are negligibly small. For the W^+W^- channels, only the hard spectra from $W^+ \rightarrow e^+\nu$ are shown. The soft component of the spectra from the W other decay modes is neglected to emphasize the small difference between the hard spectra from $W_L W_L$ and $W_T W_T$. In what follows, we disregard the effects of spin-correlations. Including the soft component, we find annihilations dominantly into W^+W^- do not provide a satisfactory spectrum.

We now enlarge the scope of our study by allowing M_{DM} to be as large as 1 TeV and allowing arbitrary weights for the following annihilation modes: e^+e^- , $\mu^+\mu^-$, $\tau^+\tau^-$, W^+W^- , ZZ , $c\bar{c}$, $b\bar{b}$, $t\bar{t}$ and hh , with a Higgs boson h of mass 120 GeV which will decay primarily into b and τ . Annihilations into Zh can be accounted for by the average of the ZZ and hh channels. The subsequent decays were computed using micrOMEGAs [20].

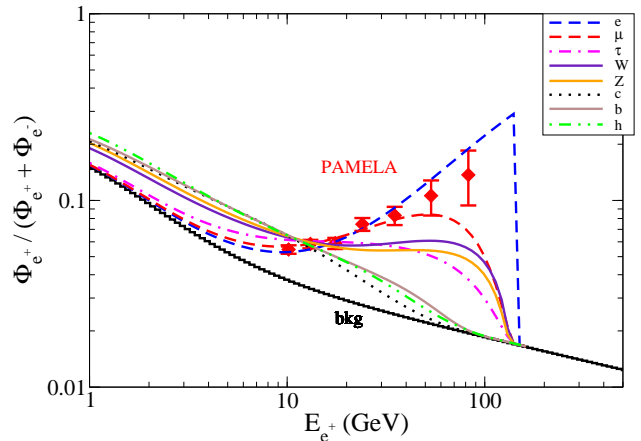


FIG. 2: Positron fraction from DM annihilation into e^+e^- , $\mu^+\mu^-$, $\tau^+\tau^-$, W^+W^- , ZZ , $c\bar{c}$, $b\bar{b}$, and hh , with a Standard Model Higgs boson h of mass 120 GeV for the Med set of propagation parameters. We have assumed that the DM annihilates into each mode with a 100% branching fraction. Accounting for the smaller boost factor, the e^+e^- mode is somewhat preferred; see Table III. The Max set yields spectra very similar to the Med set.

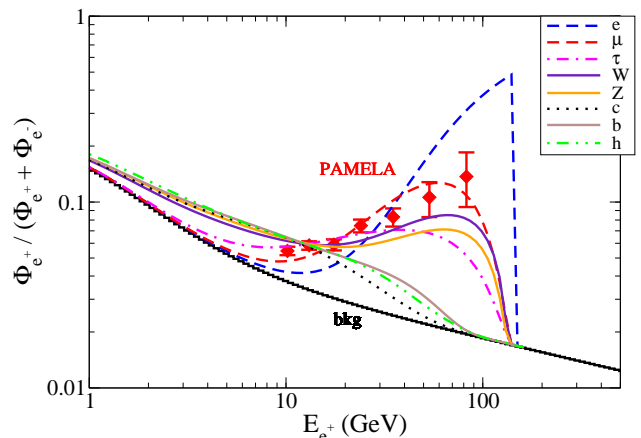


FIG. 3: Same as Fig. 2, but for the Min set of propagation parameters. The $\mu^+\mu^-$, $\tau^+\tau^-$ and W^+W^- modes are preferred; see Table III.

We denote the weights by f_{xy} , where for example, $f_{e^+e^-}$ is the weight of the e^+e^- channel. In Figs. 2 and 3, we show the positron fraction from each of these channels (except $t\bar{t}$) with $f_{xy} = 1$ for $M_{DM} = 150$ GeV. It is evident that annihilations into bosons and quarks yield too soft a spectrum, while annihilations into leptons are easily compatible with the data. The corresponding χ^2 values are listed in Table III. We have not displayed results for the Max set because it gives spectra similar to those for the Med set. Although the lowest χ^2 per degree of freedom is 2 for the Min set, we do not reject this parameter set given that uncertainties in the positron

	Med		Min	
	B	χ^2	B	χ^2
e^+e^-	30.7	5.63	71.7	94.6
$\mu^+\mu^-$	40.2	5.63	80.2	16.2
$\tau^+\tau^-$	73.0	32.2	134.6	12.0
W^+W^-	119.9	31.7	223.6	15.2
ZZ	155.7	42.6	277.9	26.9
hh	169.0	95.4	258.2	80.1
$c\bar{c}$	135.7	116.3	196.6	104.1
$b\bar{b}$	139.7	90.7	215.3	76.1
$t\bar{t}$	—	—	—	—

TABLE III: χ^2 for positron spectra from two-body annihilations of DM with mass 150 GeV for the Med and Min models of cosmic ray propagation. Results for the Max set of parameters are similar to those for the Med set. The number of degrees of freedom in each case is 6.

background have not yet been estimated. Since the Med set has a larger diffusion zone height $2L$ than the Min set, the flux of positrons incident at PAMELA is larger, thus requiring a smaller B . This explains the mode-by-mode lower boost factors for the Med set in Table III. On the other hand, the Min set has a smaller spectral index δ with relatively weaker diffusion at higher energy, resulting in a harder positron spectrum. This is evident from a comparison of the spectra in Figs. 2 and 3.

We perform a Markov Chain Monte Carlo (MCMC) analysis by varying M_{DM} between 100 GeV and 1 TeV, the boost factor B and the weights f_{xy} between 0 and 1 to determine the combination of annihilation modes that fits the positron data best; see Ref. [18] for a description of our MCMC methodology. We set the annihilation cross section to be $\langle\sigma v\rangle = 3 \times 10^{-26} \text{ cm}^{-3} \text{ s}^{-1}$, which is the typical value required to reproduce the observed relic abundance barring co-annihilations with other particles. The probability distribution of f is shown in Fig. 4. For the Med set of propagation parameters, the e^+e^- mode is preferred. For the Min set, a preference for the $\mu^+\mu^-$ and $\tau^+\tau^-$ modes is evident, and the e^+e^- mode is not favored over the non-lepton modes. In general, the data show a preference for lepton modes. The correlation matrix for the nine modes is shown graphically in Fig. 5. The 2σ contours in planes of weights for pairs of modes are plotted after marginalizing over all other modes. There is essentially no correlation between modes. It is noteworthy that while the 2σ region for the $\mu^+\mu^-$ mode and any mode (other than e^+e^-) is consistent with $(0,0)$ for the Med set, it is not so for the Min set. This is because a soft component is necessary to fit the data for the Min set. The probability distribution of B is shown in Fig. 6. For the WIMP annihilation cross section we have adopted, the boost factor is about 50 for the Med set, which is not grossly unreasonable.

From Fig. 7, we see that the range of DM masses favored by the positron data depends on the details of cosmic ray propagation. At 2σ , M_{DM} is below 215 GeV for the Med set and below 445 GeV for the Min set. The

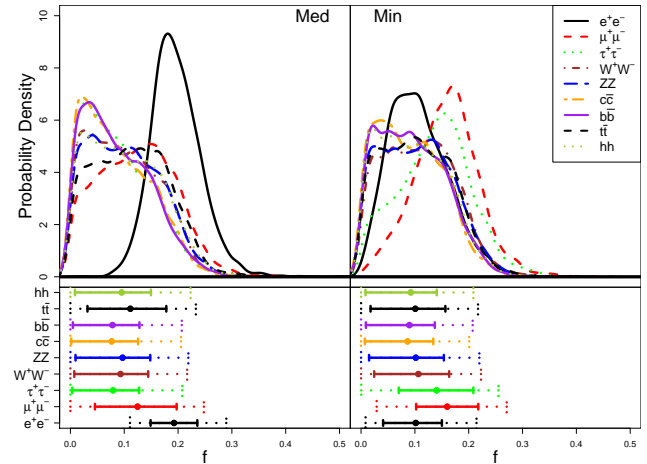


FIG. 4: The probability distribution of the weight of each channel f for the Med and Min sets. The medians, and 1σ and 2σ C. L. ranges are indicated in the lower panels.

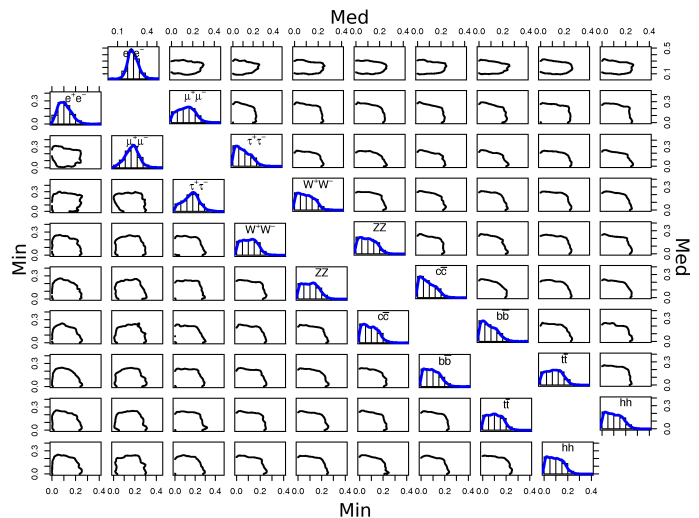


FIG. 5: A graphical representation of the correlations between modes for the Med (upper triangle) and Min (lower triangle) propagation sets. The cells along the diagonal show the probability distribution of f corresponding to the mode labeled. The contour plots show the 2σ allowed regions in planes of weights, with f of the column (row) mode along the x-axis (y-axis). No two modes are significantly correlated with each other.

correlation between B and M_{DM} in Fig. 8 shows that lighter DM particles require a smaller boost factor to explain the PAMELA positron excess. Also, with the Med set of propagation parameters, very large boost factors are avoided.

The antiproton spectrum measured by PAMELA up to 100 GeV [21] shows no deviation from the expected background [22] (which has larger uncertainties than the

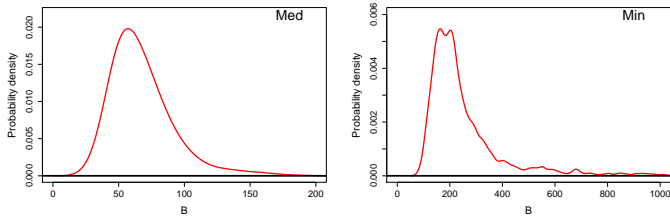


FIG. 6: The probability distribution of the boost factor B for the Med and Min propagation sets.

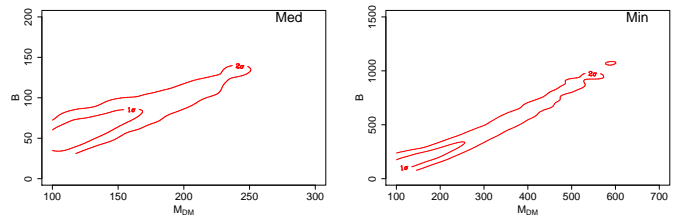


FIG. 8: The correlation between B and M_{DM} for the Med and Min propagation sets.

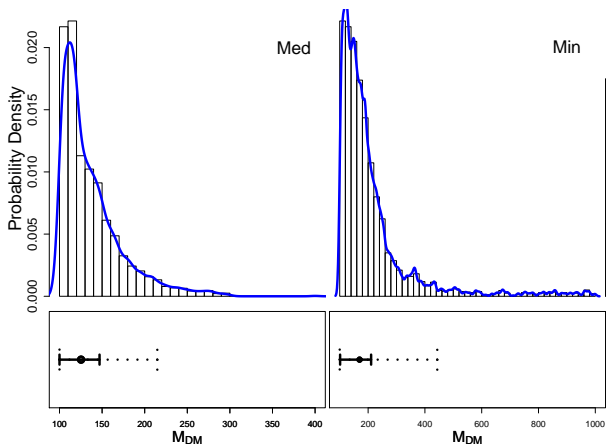


FIG. 7: The probability distribution of M_{DM} for the Med and Min sets. The medians which are 125 GeV (Med) and 170 GeV (Min), and 1σ and 2σ C. L. ranges are indicated in the lower panels.

positron background associated in part with the considerably greater propagation distance of antiprotons). Since our approach is model-independent we can not make definite statements about consistency with the cosmic antiproton data. By choosing an appropriate boost factor (which can be different from that for positrons) and appropriately modelling the propagation of antiprotons, it is easy to remain in agreement with the data. Within our approach it is also possible to have consistency by suppressing the DM annihilation branching fraction to antiquarks. As an illustration, in Fig. 9 we show the antiproton to proton flux ratio measured by PAMELA, and the theoretical expectation for the W^+W^- channel from annihilations of DM of mass 150 GeV. Boost factors for the antiproton flux below 3.3 yield agreement at the 2σ C. L. The light dashed curve shows the \bar{p}/p flux ratio if the antiproton boost factor is taken to be equal to the positron boost factor that fits the positron spectrum. Clearly, different boost factors are necessary. The 1-2 orders of magnitude difference in the e^+ and \bar{p} boost factors is a problem.

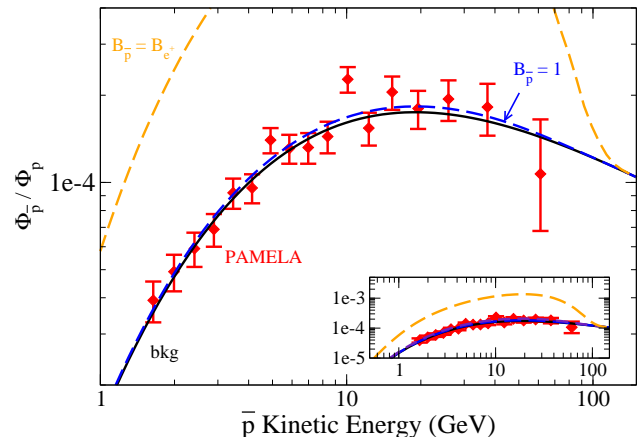


FIG. 9: The \bar{p}/p flux ratio measured by PAMELA is consistent with the expected background (solid). The dark dashed curve is the expected spectrum from DM annihilations to W^+W^- , allowing for a boost factor (equal to 1) that is different from that for positrons. The light dashed curve shows the spectrum if the boost factor for the positron fraction is applied to antiprotons; the inset shows a magnified view.

Conclusions. Our results are summarized in the figures. We have shown that the PAMELA positron excess does not favor a DM particle of a particular spin. The data do not discriminate between positron spectra from direct production and from secondary decays of polarized W bosons. However, PAMELA is expected to collect positrons up to about 270 GeV. With those data it should be possible to draw stronger conclusions. If the data show a line, popular SUSY models will be in danger of being excluded and models with extra dimensions and collective symmetry breaking will gain support since they have spin-1 DM. Models with Dirac fermions as DM will also be viable. On the other hand if the data roll-over smoothly near the endpoint, and are fit well by positrons from transversely polarized W bosons, SUSY will be indicated. If positrons from longitudinally polarized W bosons are preferred by the data, neutralino DM will be in jeopardy, and the DM candidates of mUED and LHT will be preferred. To make such fine distinctions in spectral shapes will require much larger datasets

from PAMELA and the Alpha Magnetic Spectrometer.

By considering nine different two-body annihilation channels with arbitrary weights, for dark matter lighter than 1 TeV, we found that lepton modes are generally preferred by the positron data, and which lepton modes are favored depends on the details of cosmic ray propagation. The $\mu^+\mu^-$ and $\tau^+\tau^-$ modes fit the data better than the obvious e^+e^- mode for the Min set. Also, we found that dark matter masses selected by the data depend on the propagation model. The 2σ upper limit is 215 GeV for the Med set of propagation parameters and 445 GeV for the Min set. Results for the Max set are similar to those for the Mid set.

It is important to bear in mind that although astrophysical processes are expected to produce a positron background that falls with energy, it may still be that astrophysical sources such as pulsars could mimic the putative DM signal. Confidence in the DM interpretation will be strengthened by signals in other experiments, involving both direct and indirect detection methods.

Acknowledgments. This research was supported by DOE Grant Nos. DE-FG02-04ER41308, DE-FG02-95ER40896, DE-FG02-84ER40173 and DE-AC02-06CH11357, by NSF Grant No. PHY-0544278, and by the Wisconsin Alumni Research Foundation.

-
- [1] T. Appelquist, H. C. Cheng and B. A. Dobrescu, Phys. Rev. D **64**, 035002 (2001) [arXiv:hep-ph/0012100].
 - [2] H. C. Cheng and I. Low, JHEP **0309**, 051 (2003) [arXiv:hep-ph/0308199].
 - [3] V. Barger *et al.*, Phys. Rev. D **77**, 035005 (2008) [arXiv:0706.4311 [hep-ph]].
 - [4] O. Adriani *et al.*, arXiv:0810.4995 [astro-ph].
 - [5] L. Bergstrom, T. Bringmann and J. Edsjo, arXiv:0808.3725 [astro-ph].
 - [6] M. Cirelli and A. Strumia, arXiv:0808.3867 [astro-ph].
 - [7] S. Torii *et al.*, arXiv:0809.0760 [astro-ph].
 - [8] I. V. Moskalenko and A. W. Strong, Astrophys. J. **493**, 694 (1998) [arXiv:astro-ph/9710124].
 - [9] E. A. Baltz and J. Edsjo, Phys. Rev. D **59**, 023511 (1998) [arXiv:astro-ph/9808243].
 - [10] M. Cirelli, R. Franceschini and A. Strumia, Nucl. Phys. B **800**, 204 (2008) [arXiv:0802.3378 [hep-ph]].
 - [11] J. Hisano, S. Matsumoto, O. Saito and M. Senami, Phys. Rev. D **73**, 055004 (2006) [arXiv:hep-ph/0511118].
 - [12] T. Delahaye, R. Lineros, F. Donato, N. Fornengo and P. Salati, Phys. Rev. D **77**, 063527 (2008) [arXiv:0712.2312 [astro-ph]].
 - [13] J. N. Bahcall and R. M. Soneira, Astrophys. J. Suppl. **44**, 73 (1980).
 - [14] D. Maurin, F. Donato, R. Taillet and P. Salati, Astrophys. J. **555**, 585 (2001) [arXiv:astro-ph/0101231].
 - [15] J. Lavalle, Q. Yuan, D. Maurin and X. J. Bi, arXiv:0709.3634 [astro-ph].
 - [16] G. Servant and T. M. P. Tait, Nucl. Phys. B **650**, 391 (2003) [arXiv:hep-ph/0206071].
 - [17] A. Birkedal, A. Noble, M. Perelstein and A. Spray, Phys. Rev. D **74**, 035002 (2006) [arXiv:hep-ph/0603077].
 - [18] V. Barger, W. Y. Keung and G. Shaughnessy, Phys. Rev. D **78**, 056007 (2008) [arXiv:0806.1962 [hep-ph]].
 - [19] V. Barger, W. Y. Keung, G. Shaughnessy and A. Tregre, Phys. Rev. D **76**, 095008 (2007) [arXiv:0708.1325 [hep-ph]].
 - [20] G. Belanger, F. Boudjema, A. Pukhov and A. Semenov, arXiv:0803.2360 [hep-ph]; Comput. Phys. Commun. **176**, 367 (2007) [arXiv:hep-ph/0607059].
 - [21] O. Adriani *et al.*, arXiv:0810.4994 [astro-ph].
 - [22] T. Bringmann and P. Salati, Phys. Rev. D **75**, 083006 (2007) [arXiv:astro-ph/0612514].